2001074926
529448
24 Pgs
TR/IN/26

Microprobe Evaluations of Grain Boundary Segregation in KM4 and IN100

T.P. Gabb
Glenn Research Center, Cleveland, Ohio

J.W. Smith
Cleveland State University, Cleveland, Ohio

January 2001

Since its founding, NASA has been dedicated to the advancement of aeronautics and space science. The NASA Scientific and Technical Information (STI) Program Office plays a key part in helping NASA maintain this important role.

The NASA STI Program Office is operated by Langley Research Center, the Lead Center for NASA's scientific and technical information. The NASA STI Program Office provides access to the NASA STI Database, the largest collection of aeronautical and space science STI in the world. The Program Office is also NASA's institutional mechanism for disseminating the results of its research and development activities. These results are published by NASA in the NASA STI Report Series, which includes the following report types:

- TECHNICAL PUBLICATION. Reports of completed research or a major significant phase of research that present the results of NASA programs and include extensive data or theoretical analysis. Includes compilations of significant scientific and technical data and information deemed to be of continuing reference value. NASA's counterpart of peer-reviewed formal professional papers but has less stringent limitations on manuscript length and extent of graphic presentations.

- TECHNICAL MEMORANDUM. Scientific and technical findings that are preliminary or of specialized interest, e.g., quick release reports, working papers, and bibliographies that contain minimal annotation. Does not contain extensive analysis.

- CONTRACTOR REPORT. Scientific and technical findings by NASA-sponsored contractors and grantees.

- CONFERENCE PUBLICATION. Collected papers from scientific and technical conferences, symposia, seminars, or other meetings sponsored or cosponsored by NASA.

- SPECIAL PUBLICATION. Scientific, technical, or historical information from NASA programs, projects, and missions, often concerned with subjects having substantial public interest.

- TECHNICAL TRANSLATION. English-language translations of foreign scientific and technical material pertinent to NASA's mission.

Specialized services that complement the STI Program Office's diverse offerings include creating custom thesauri, building customized data bases, organizing and publishing research results . . . even providing videos.

For more information about the NASA STI Program Office, see the following:

- Access the NASA STI Program Home Page at *http://www.sti.nasa.gov*

- E-mail your question via the Internet to help@sti.nasa.gov

- Fax your question to the NASA Access Help Desk at 301–621–0134

- Telephone the NASA Access Help Desk at 301–621–0390

- Write to:
  NASA Access Help Desk
  NASA Center for AeroSpace Information
  7121 Standard Drive
  Hanover, MD 21076

Microprobe Evaluations of Grain Boundary Segregation in KM4 and IN100

T.P. Gabb
Glenn Research Center, Cleveland, Ohio

J.W. Smith
Cleveland State University, Cleveland, Ohio

National Aeronautics and
Space Administration

Glenn Research Center

MICROPROBE EVALUATIONS OF GRAIN BOUNDARY SEGREGATION IN KM4 AND IN100

T. P. Gabb and J. W. Smith

Introduction

HSCT compressor and turbine disks will be subjected to cyclic dwells at maximum load and strain during supercruise. Cyclic dwells have been shown to promote cracking along grain boundaries in many modern nickel-base disk alloys (ref. 1-5), due to creep-fatigue-environment interactions (ref. 1). Comparison dwell fatigue crack growth tests of the EPM disk program alloy KM4 performed in air and vacuum at 1200°F (ref. 5) indicate fatigue-environment interactions could predominate in the long dwells anticipated in HSCT applications. It is therefore important to understand the local chemistry of the grain boundaries and identify any chemical segregation along the grain boundaries. Microstructural investigations of the current HSR-EPM disk alloys KM4 and IN100 using transmission electron microscopy (TEM) at NASA LeRC (ref. 6) have indicated very fine $Cr_{23}C_6$ carbides of 200-1000Å diameter tend to predominate along the grain boundaries, accompanied by scattered coarser MC carbides of 1500-6000Å diameter, and $(Mo,Cr)_3B_2$ borides of 5000-10000Å diameter. Energy dispersive x-ray chemical analyses in the TEM at a resolution of about 0.1 μm could detect no consistent differences in the compositions of γ or γ' with respect to their distances from the grain boundaries. However, these analyses were hampered by foil thickness variations, foil distortions, and detector limitations.

The objective of this study was to evaluate the degree of segregation present at the grain boundaries in two current EPM disk program alloys, KM4 and IN100, using wavelength dispersive x-ray (WDX) chemical analyses in the microprobe. The microprobe is capable of quantitative chemical analyses at a resolution of about 1.5 μm. This would enable quantitative chemical comparisons across a larger scale.

Experimental Procedure

KM4 has a nominal composition (ref. 7) of Ni-12Cr-18Co-4Ti-4Al-4Mo-2Nb-.03C-.03B-.03Zr(wt.%). IN100 has a nominal composition (ref. 7) of Ni-12.4Cr-18.5Co-4.3Ti-5.0Al-3.2Mo-0.8V-.07C-.02B-.06Zr(wt.%). Both alloys had a nominal grain size of ASTM 6-7. The examination was performed in an ARL-SEMQ electron microprobe on metallographic cross sections of each alloy coated with approximately 200Å of carbon. The microprobe was consistently operated at an accelerating voltage of 20kV and a beam current of 18 nano-amps for all measurements. This produced an accelerated volume of approximately 1.5 μm in diameter, which would typically contain the γ, cooling γ', and aging γ' phases in these alloys. Conventional WDX analog x-ray mapping and x-ray line scan profiles failed to define any significant chemical anomalies across the grain boundaries, other than scattered boride particles. A more sensitive technique available is digital point x-ray mapping, a part of the microprobe automation program. Counting statistics are greatly improved by this method, which allows the imaging of subtle variations in chemistry. Count rates in the digital maps are delineated by a gradient of false color, the extremes being black (lowest counts detected) and white (highest counts detected). This analysis was performed on typical areas of both samples at a magnifications of about 2000-4000X, which would define a number of

grain boundaries and still maintain x-ray definition. In each x-ray image, counts were acquired for 0.3 sec/point over a 200 X 200 point grid. The completed digital point maps were then used as a guide to perform conventional quantitative analyses at points in the same area.

A lithium fluoride spectrometer crystal (LiF, 2d = 4.0267Å) was employed for chromium, cobalt, nickel, and titanium detection. Aluminum was detected using a thallium acid pthalate crystal (TAP, 2d = 25.75Å), while a pentaerythritol crystal (PET, 2d = 8.742Å) was used for molybdenum. A layered synthetic material crystal (LSM200, 2d = 197.4Å) was used for boron detection. The pure element was used as a standard in each case.

Results and Discussion
1. KM4

Figure 1a illustrates a number of grains in a typical field for KM4. The digital point map for boron corresponding to this image illustrated a distinct boron enrichment along most boundaries. TEM analyses had only indicated scattered borides, therefore the higher boron generally observed along the grain boundaries was apparently in solid solution. An image at higher magnification is provided along with boron, chromium, and molybdenum maps in Figure 2. High molybdenum and boron concentrations often coincided at scattered points along the grain boundaries, consistent with $(Mo,Cr)_3B_2$ borides detected previously in transmission electron microscopy (ref. 6). Some evidence of fluctuating chrome enrichment along the grain boundaries is apparent, possibly due to the very fine $Cr_{23}C_6$ carbides observed in TEM, which cannot be resolved in the microprobe.

Quantitative point analyses of the points indicated in Figure 3 are presented in Table 1. The elements Al, Ni, Co, Cr, and Ti were chosen for this analysis, due to spectrometer limitations in the number of elements which can measured in a timely manner and the poor counting statistics of the minor elements C, B, and Zr. The data in Table 1 represents no corrections for the unanalyzed elements Mo, B, Zr, and C. These relatively minor ZAF corrections are included in Table 2. The averaged values in Table 4 indicate a slight enrichment of Co and Cr at a statistical confidence of 95%. The higher standard deviations of the grain boundary measurements may be associated with variability of the grain boundary orientation within the 1.5 μm diameter volume accelerated in these measurements. The chromium levels may be variably increased at the grain boundary due to $Cr_{23}C_6$ carbides within the accelerated volume, and both Cr and Co levels could be increased by the presence of more γ phase along the grain boundaries than within grains.

2. IN100

A typical area of IN100 selected for digital point mapping of boron, chromium, and molybdenum is illustrated in Fig. 4. Large secondary γ' precipitates within the grains and along the grain boundaries are indicated by the arrows in the analog backscattered electron images. The area imaged in the digital micrograph (Fig. 4b) corresponds to the digital point maps in Fig. 4c-4e. Fig. 4c-4e illustrates that boron and molybdenum are generally concentrated in distinct particles less than 1μm in diameter, probably $(Mo,Cr)_3B_2$ borides. There is only a slight suggestion of boron enrichment along most of the grain boundaries, less than in KM4. Chromium is enriched along the grain boundaries, but there is no evidence of a continuous gradient from the grain interior. In addition, the map suggests that

the level of chromium fluctuates along the grain boundary as in KM4, possibly due to $Cr_{23}C_6$ carbides.

A series of quantitative point analyses were performed in a specific area of IN100 as before. The region selected for the analyses is shown in Fig. 5. The insert defines the map area illustrated in Figures 5b (chromium) and Fig. 5c (cobalt). The point locations are illustrated in the micrograph of Fig. 5d. The quantitative point analyses are presented in Table 4, incorporating the minor ZAF corrections for the unanalyzed elements Mo, V, B, Zr, and C. Averaged values in Table 4 again indicate slight enrichments of Cr and Co, at a statistical confidence of 95%. The higher variability of the grain boundary measurements may again be associated with variations in the grain boundary orientation and $Cr_{23}C_6$ carbide content within the accelerated volume.

Analysis points 16 and 18 are centered in two large secondary γ' precipitates aligned along a grain boundary. These analysis points give the approximate composition of the secondary γ', as the size of these particles appears to exceed the accelerated volume in the measurements. The composition of this secondary γ' indicates higher chromium content than that typically reported elsewhere (ref. 8), as shown in the comparison of Table 4. The higher chromium could have a significant influence on the environmental resistance of this γ' phase and the grain boundaries. This result is still subject to some concern about the depth of these particles with respect to the accelerated volume. Bulk chemistry measurements of filtered γ' phase extractions may offer an alternative method to confirm this finding.

Summary and Conclusions

Microprobe evaluations disclosed no large scale concentration gradients at the grain boundaries in either KM4 or IN100, within the resolution limitations of this instrument. Evidence of general boron enrichment along the grain boundaries was observed in KM4, but only slight evidence of this was observed in IN100. Quantitative point analyses suggest slight Cr and Co increases at the grain boundaries of both alloys. This could be attributed to the presence at grain boundaries of very fine $Cr_{23}C_6$ carbides, and higher γ phase content, respectively. However, these features are not resolvable in the microprobe. Quantitative analyses of coarse secondary γ' at the grain boundaries of IN100 suggested relatively high Cr content in this γ'. This needs to be confirmed, using wet chemistry of carefully filtered secondary γ' phase extractions.

References
1. R. M. Pelloux and J. S. Huang, "Creep-Fatigue-Environment Interactions in Astroloy", in Creep-Fatigue-Environment Interactions, ed. by R. M. Pelloux and N. S. Stoloff, The Metallurgical Society of AIME, Warrendale, PA, 1980, pp.151-164.
2. J. Schirra, "Specimen Characterization-SPLCF", in HSR-EPM Coord. Memo. No. 05-G-94032119, ed. by E. S. Huron, March 21, 1994, pp. 6.6-6.29.
3. E. S. Huron, "Fatigue Crack Growth Fractography Details", in HSR-EPM Coord. Memo. No. 05-G-94072722, ed. by E. S. Huron and K. R. Bain, July 27, 1994, pp. H-9 to H13.
4. T. P. Gabb and J. Gayda, "Effect of Tensile Strain Dwells on Strain Controlled LCF Response at 1200°F", in HSR-EPM Coord. Memo. No. 05G-020995100, ed. by R. D. Kissinger, January 18, 1995.
5. J. Telesman, "Preliminary Observations of the In Situ FCG Behavior of KM4 at 1200°F

in Vacuum", in HSR-EPM Coor. Memo. No. 05-P94092210, ed. J. Heine, September 22, 1994, pp. 12-41.

6. T. P. Gabb, A. Garg, and D. R. Ellis, "Characterization of Grain Boundaries in HSR-EPM Disk Alloys", in HSR-EPM Coord. Memo. No. 05-P94060310, ed. by J. Schirra, May 18, 1994.

7. HSR-EPM Coordination Memorandum No. 05-P93060808, ed. by D. F. Paulonis, June 8, 1993.

8. C. T. Sims, "The Role of Refractory Metals in Austenitic Superalloys," 6th Plansee Seminar, Reutte, Austria, June, 1968, in Superalloys II, ed. C. T. Sims, N. S. Stoloff, W. C. Hagel, John Wiley & Sons, New York, 1987, p. 108.

Alloy and Location	Al	Ni	Co	Cr	Ti	No.
	wt. %, Mean ± Standard Deviation					Points
KM4						
Within Grains	3.145±.049	54.311±.294	18.453±.074	12.254±.077	4.015±.072	9
Grain Boundaries	2.999±.187	52.883±1.32	18.679±.245	12.735±.348	4.109±.228	9
IN100						
Within Grains	5.114±.034	54.321±.343	19.800±.131	13.458±.156	3.975±.137	10
Grain Boundaries	5.008±.078	53.525±.657	20.184±.299	13.867±.337	3.897±.391	6
G.B. Secondary γ'	5.876±.180	58.319±1.64	17.439±.537	9.913±1.004	5.415±.228	2

Table 4. Averaged quantitative point analysis results.

Alloy	Al	Ni	Co	Cr	Ti	Other
			at.%			
IN100	12.03	54.86	16.34	10.54	6.23	-
Udimet 520	-	73.89	7.22	4.31	9.49	1.8Mo,0.31W

Table 5. Comparison of the compositions (at.%) of the secondary γ' along the grain boundaries of IN100 with the grain boundary γ' (ref. 8) of a higher chromium alloy, Udimet 520 (Ni-19Cr-12Co-6Mo-1W-2Al-3Ti-.05C-.005B, wt.%).
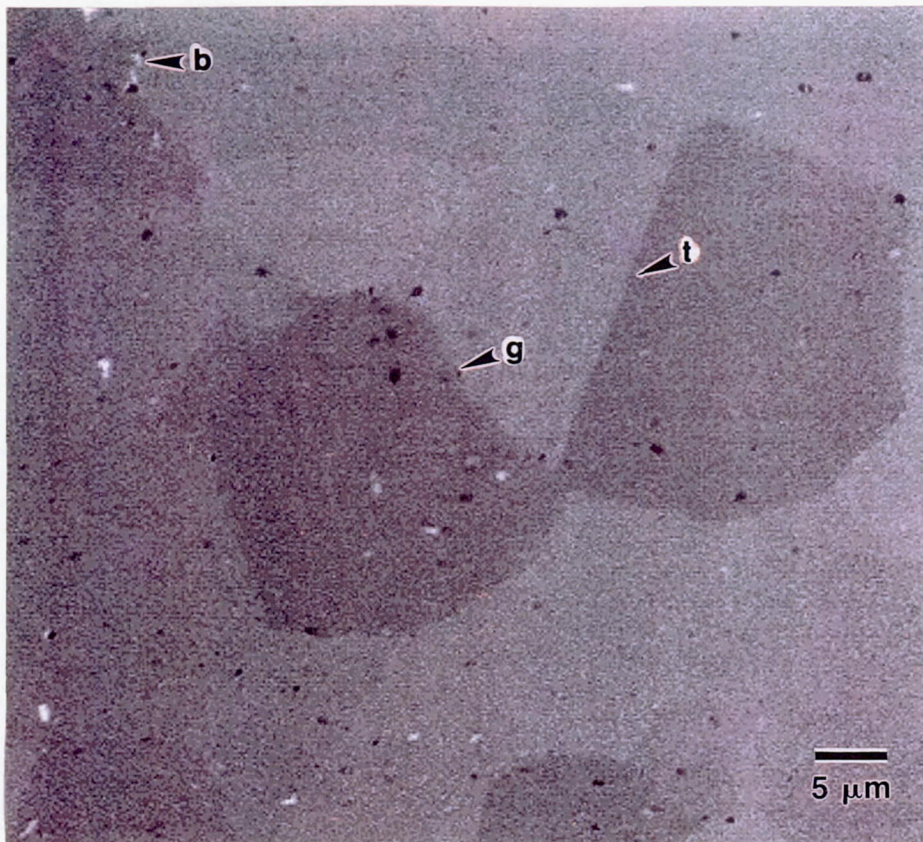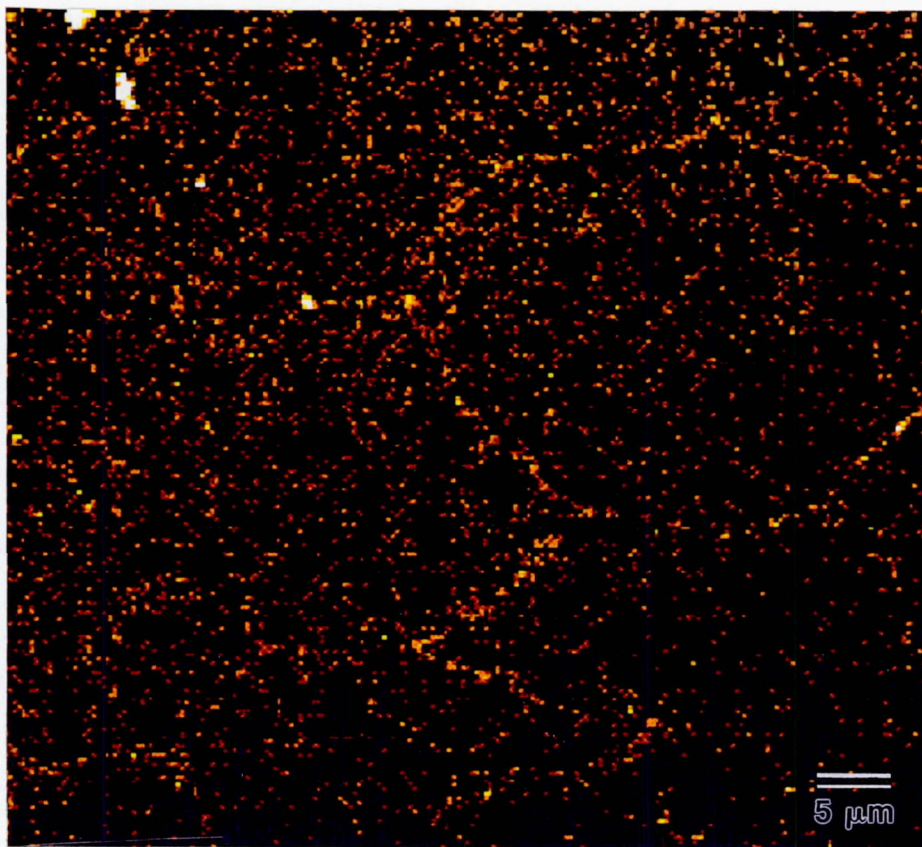
Figure 1. Typical microstructure of KM4: a. backscattered electron (BSE) image showing grain boundary (g), twin boundary (t), boride (b); b. digital point map of boron distribution showing boron enrichment along grain boundaries.
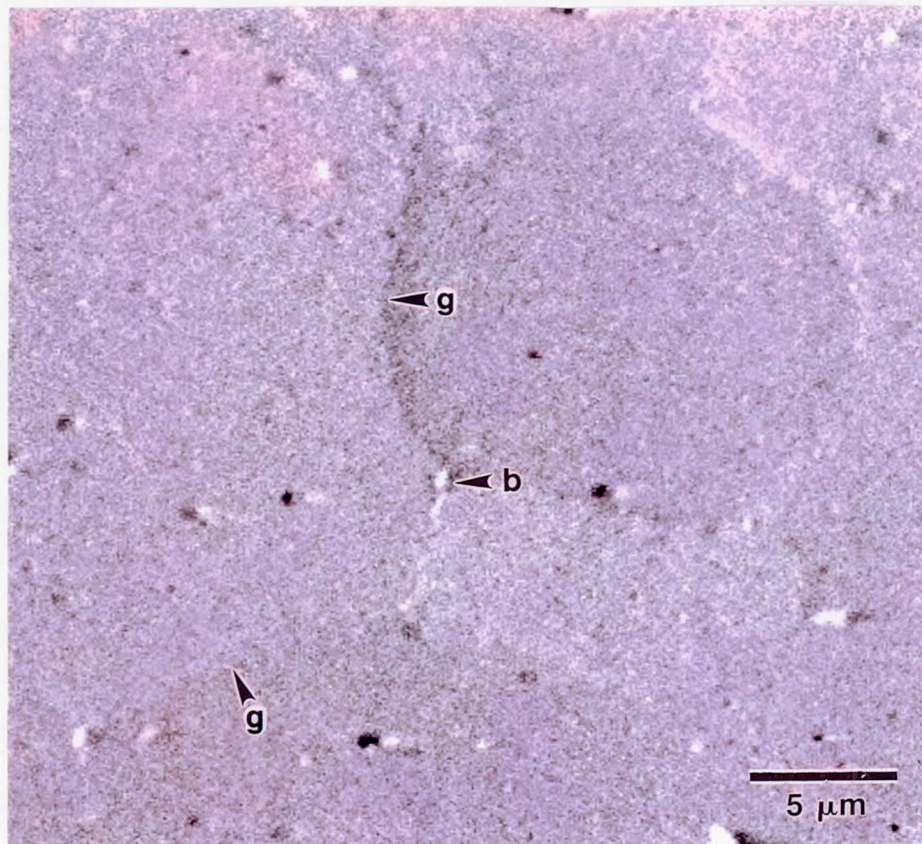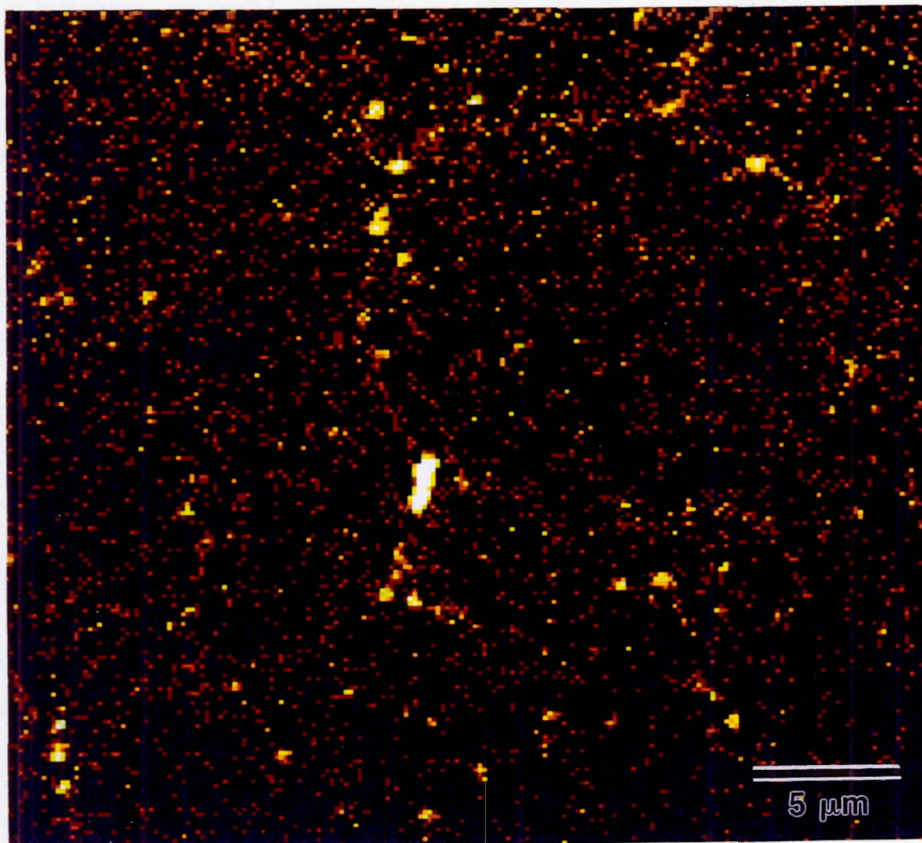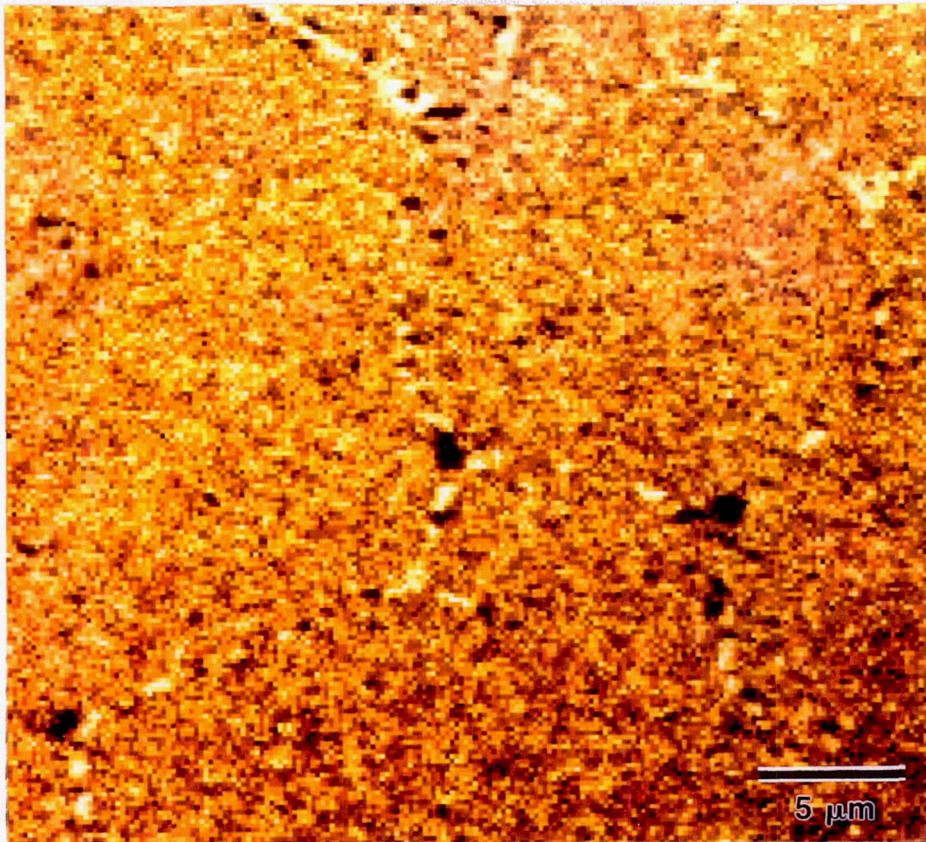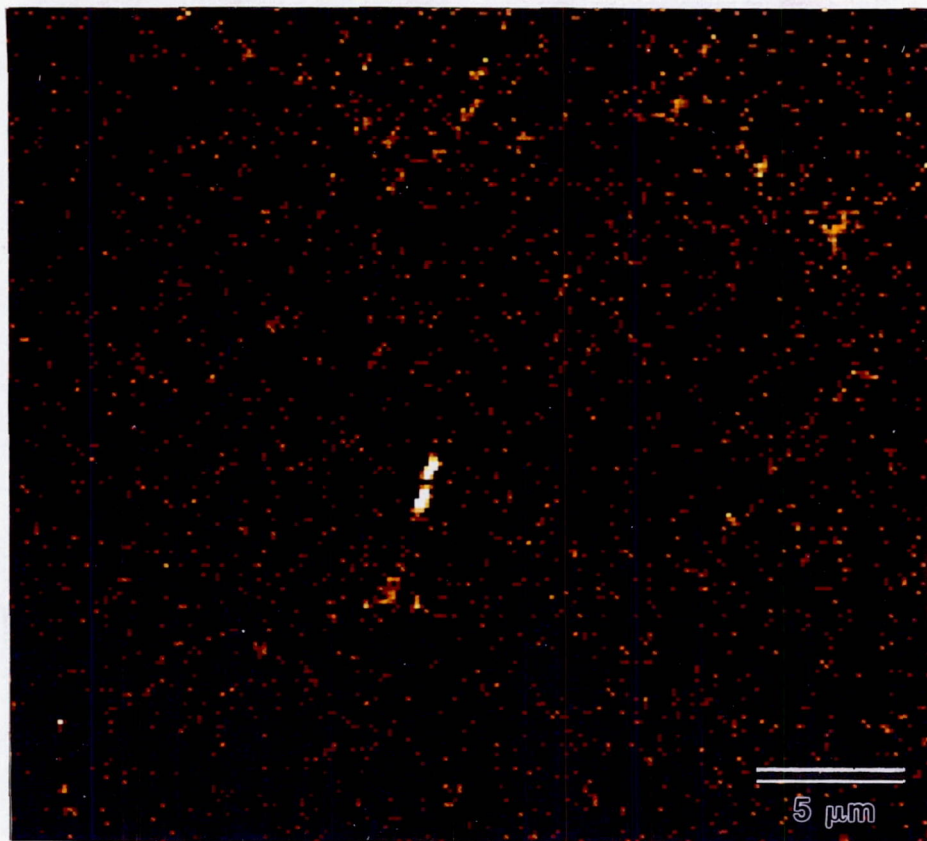
Figure 2. Higher magnification image of KM4 showing probable $(Mo,Cr)_3B_2$ boride particles: a. digital BSE image showing grain boundaries (g), boride (b); b. digital point map of boron distribution.
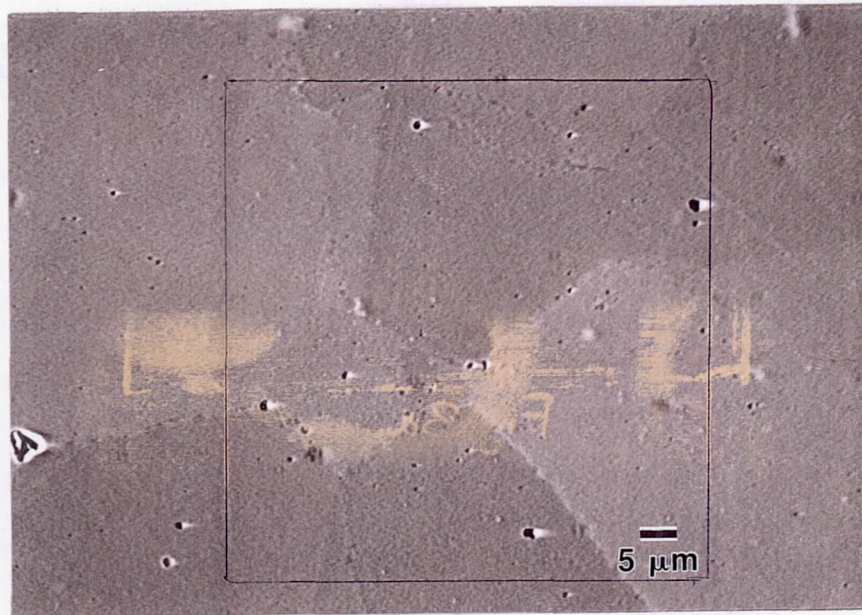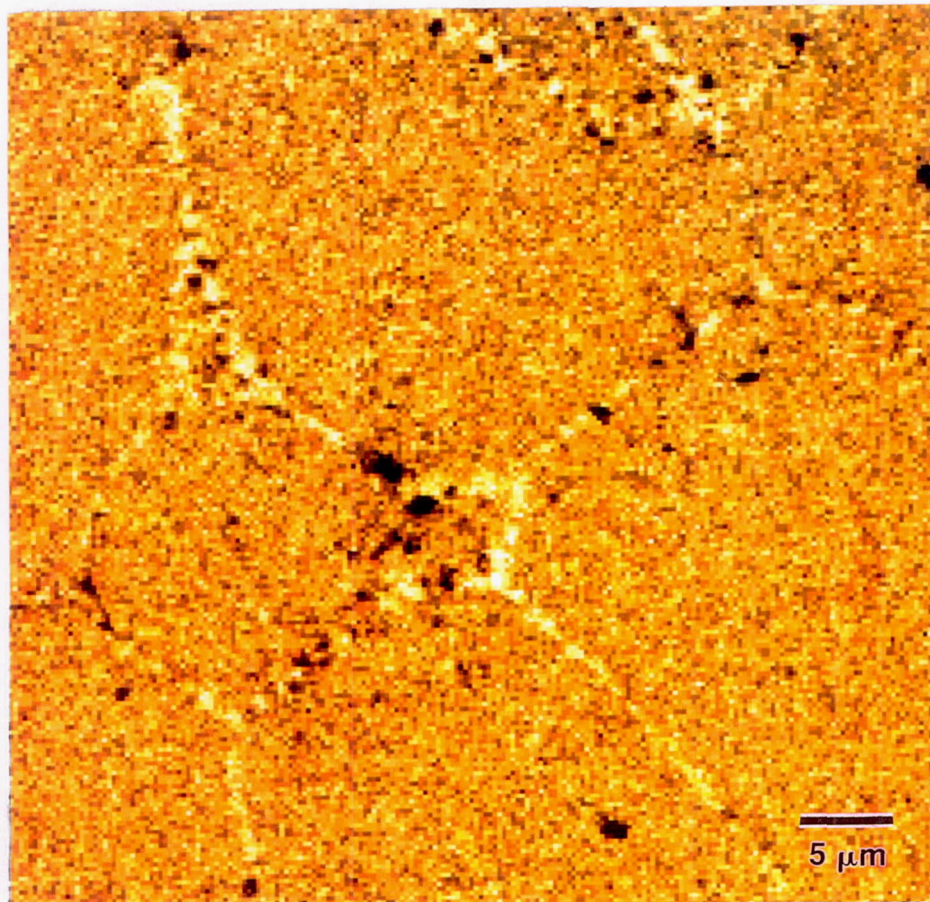
c.

d.

Fig. 2. (cont.) c. Digital point map of chromium distribution; d. digital point map of molybdenum distribution.

8

Figure 3. Area selected for quantitative point analyses of KM4: a. BSE image with insert showing mapped area; b. digital point map of chromium distribution.
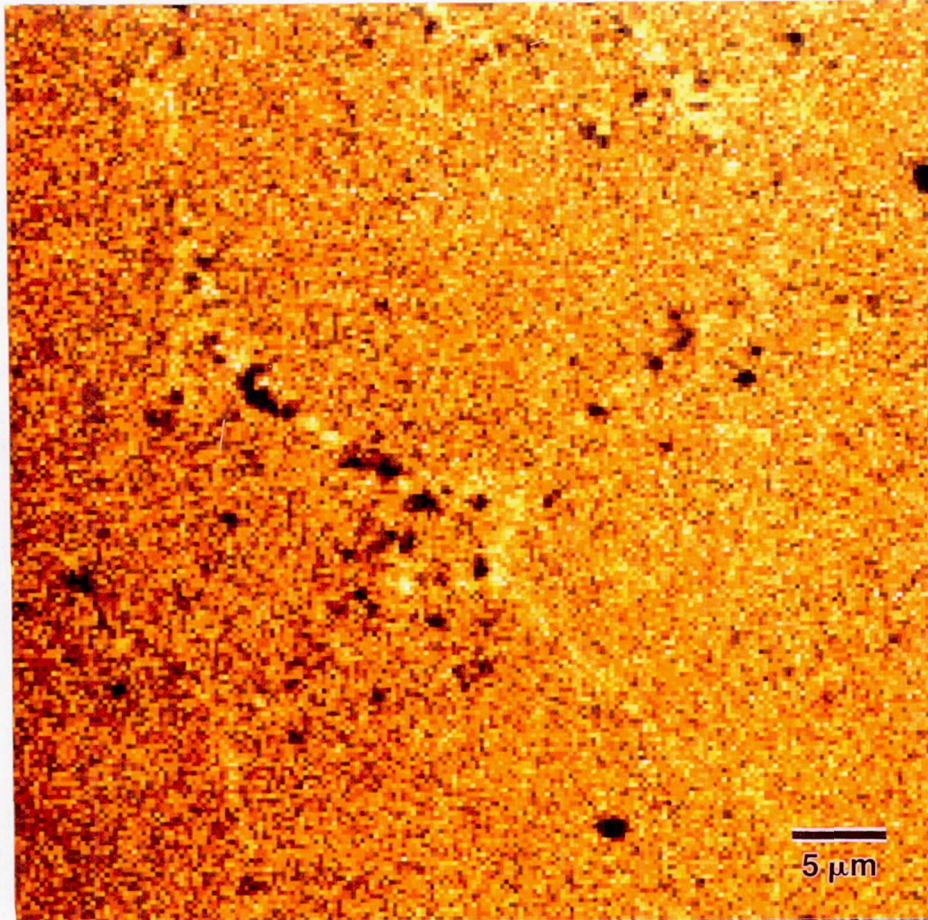
Fig. 3. (cont.) c. Digital point map of cobalt distribution.

Table 1. Quantitative point analyses results for KM4, *-grain boundary point.

| Analysis Point	Al	Ni	Co	Cr	Ti	Totals
1	3.147	54.775	18.573	12.167	4.037	92.700
2	3.180	54.827	18.595	12.160	4.032	92.794
3	3.224	54.752	18.675	12.156	3.935	92.742
4	3.226	54.866	18.536	12.289	4.017	92.934
* 5	3.115	53.706	18.809	12.777	3.824	92.231
* 6	3.124	53.249	18.943	12.880	3.816	92.012
* 7	2.827	51.850	18.994	12.837	4.158	90.666
8	3.176	54.831	18.578	12.182	3.855	92.622
9	3.305	54.756	18.518	12.019	4.047	92.644
* 10	3.366	55.022	18.327	11.831	4.059	92.605
11	3.203	54.941	18.418	12.186	4.011	92.759
* 12	3.182	54.444	18.557	12.428	3.946	92.556
* 13	2.764	50.619	18.909	13.004	4.358	89.654
* 14	2.952	53.087	19.027	12.716	4.350	92.133
* 15	3.085	53.362	19.013	12.680	4.281	92.421
16	3.225	53.994	18.608	12.169	3.876	91.872
17	3.279	54.436	18.631	12.062	3.991	92.399
* 18	3.204	53.918	18.609	12.553	3.839	92.123
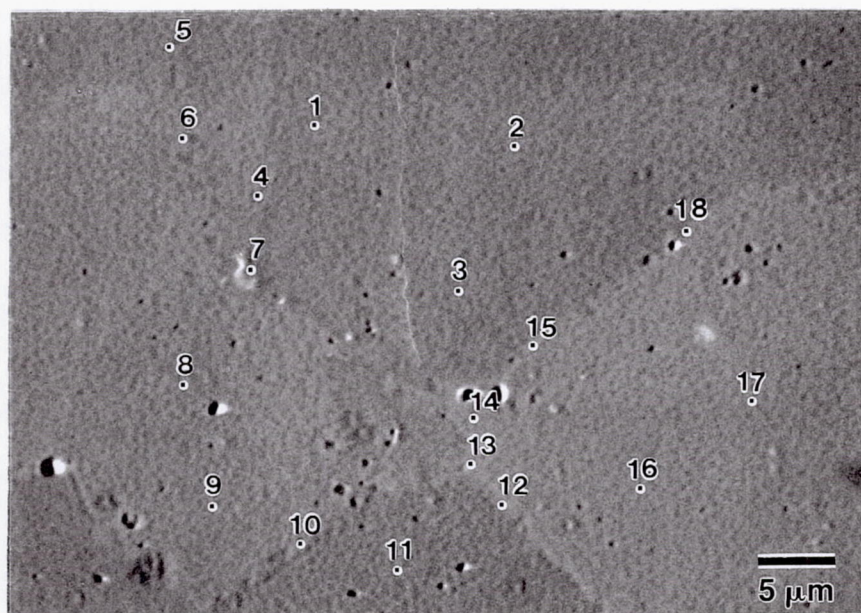
Fig. 3 (cont.) d. Digital BSE image with the locations of quantitative point analyses.

Table 2. Quantitative point analyses results for KM4, incorporating ZAF corrections for the unanalyzed elements 4.0Mo, 2.0Nb, 0.03C, 0.03B, and 0.03Zr, *-grain boundary point.

| Analysis Point	Al	Ni	Co	Cr	Ti	Totals
1	3.076	54.400	18.456	12.266	4.075	98.363
2	3.108	54.451	18.478	12.259	4.070	98.456
3	3.151	54.377	18.558	12.256	3.972	98.403
4	3.153	54.491	18.419	12.389	4.054	98.596
* 5	3.044	53.336	18.690	12.880	3.861	97.901
* 6	3.053	52.882	18.823	12.984	3.853	97.684
* 7	2.761	51.489	18.872	12.939	4.199	96.349
8	3.103	54.455	18.461	12.282	3.892	98.284
9	3.230	54.380	18.401	12.117	4.085	98.302
* 10	3.290	54.643	18.211	11.928	4.097	98.258
11	3.130	54.565	18.302	12.285	4.049	98.420
* 12	3.109	54.070	18.439	12.528	3.983	98.220
* 13	2.700	50.262	18.786	13.104	4.402	95.343
* 14	2.885	52.722	18.907	12.815	4.392	97.811
* 15	3.015	52.996	18.893	12.779	4.322	98.094
16	3.151	53.621	18.490	12.269	3.913	97.534
17	3.204	54.062	18.513	12.161	4.029	98.058
* 18	3.131	53.546	18.491	12.655	3.875	97.788
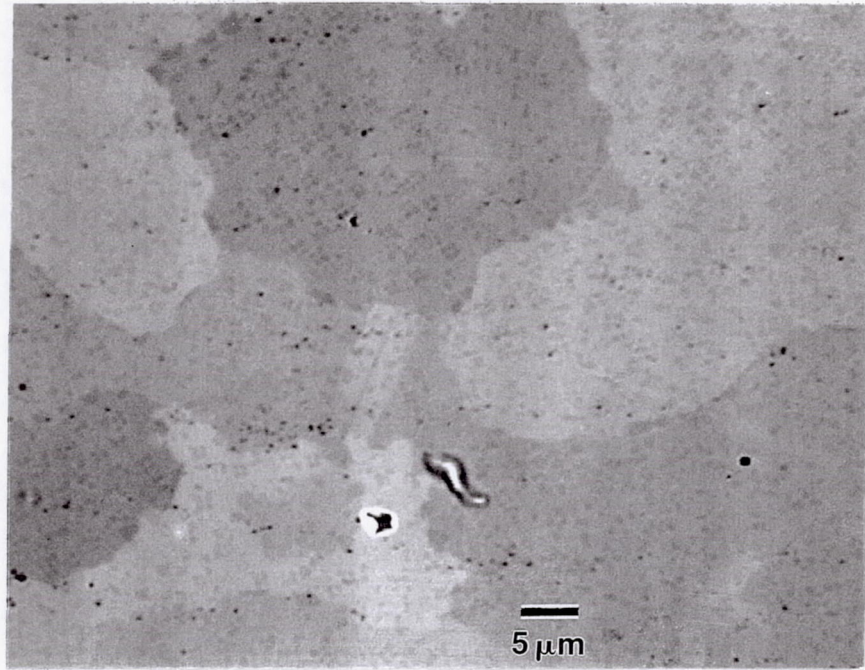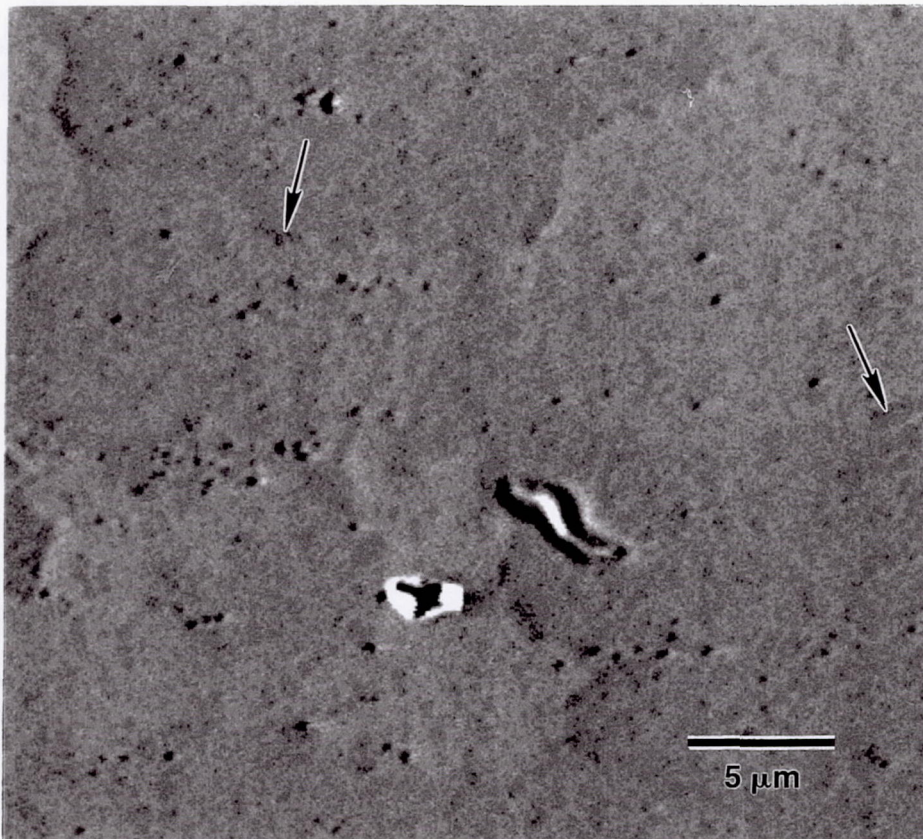
Figure 4. Typical microstructure of IN100: a. analog BSE image; b. magnified digital BSE image with arrows indicating coarse secondary γ' precipitates at grain boundaries;

13
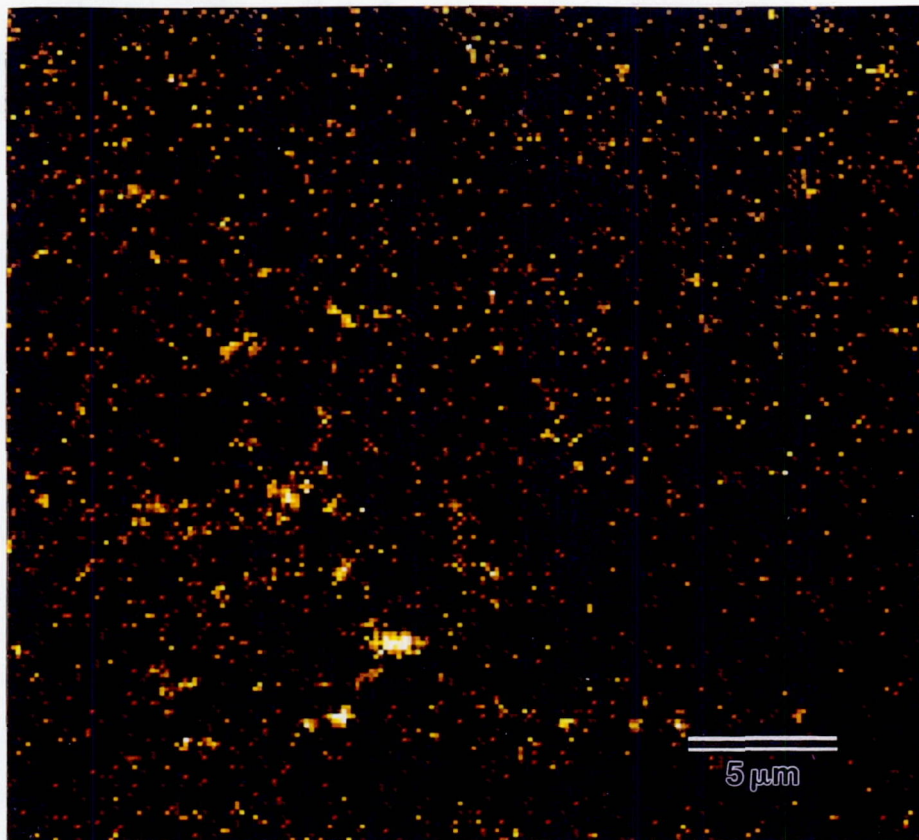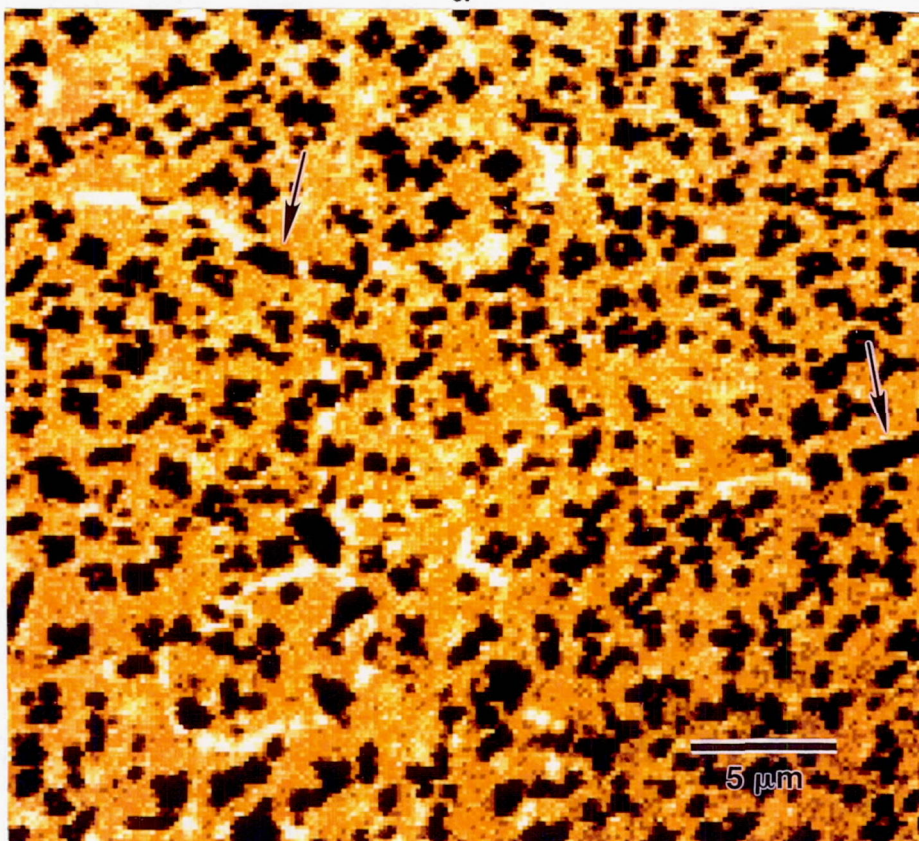
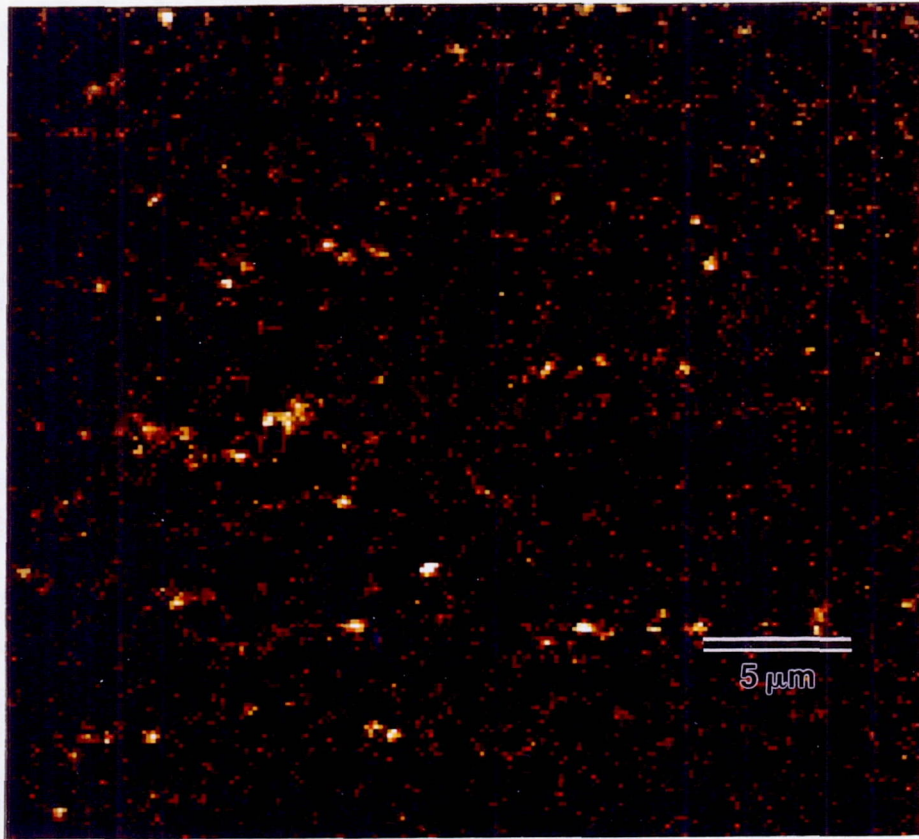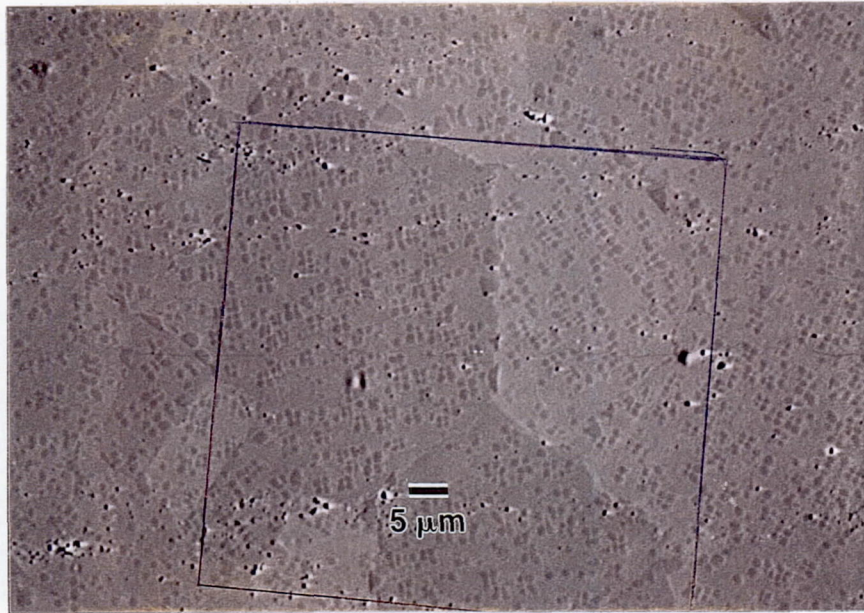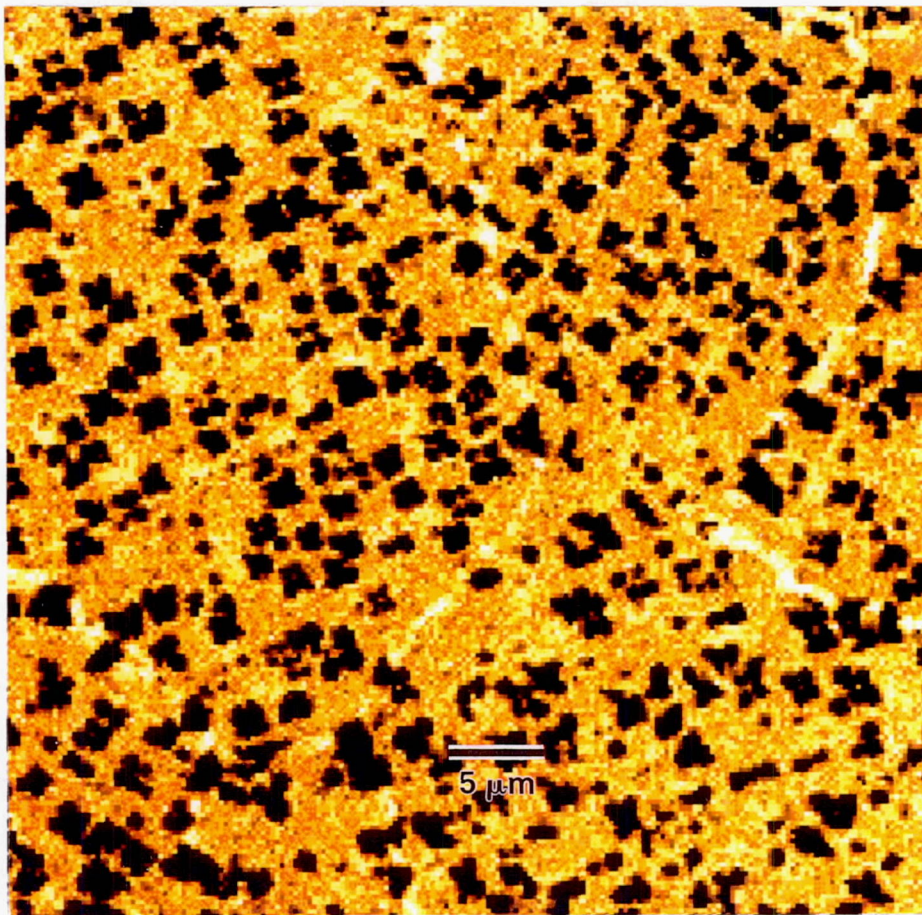Fig. 4. (cont.) c. Digital point map of boron distribution; d. digital point map of chromium distribution.

Fig. 4. (cont.) e. Digital point map of molybdenum distribution.

Figure 5. Area selected for quantitative point analyses of IN100: a. BSE image with insert showing mapped area; b. digital point map of chromium distribution.
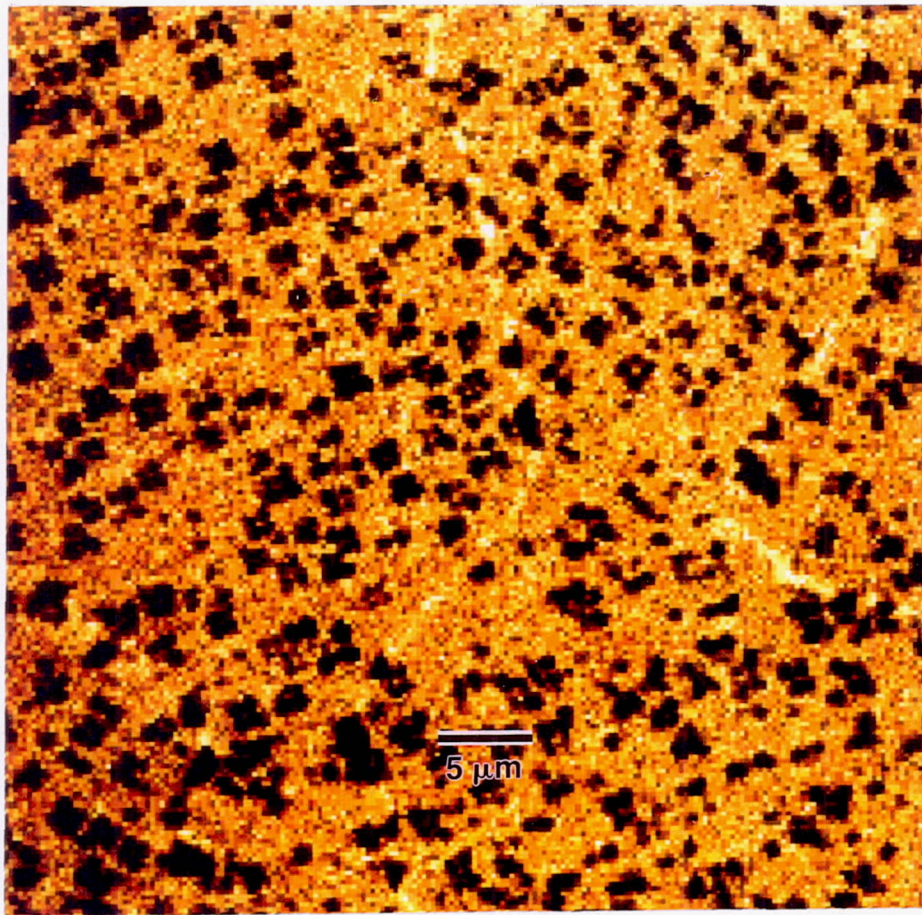
Fig. 5. (cont.) c. Digital point map of cobalt distribution.

Table 3. Quantitative point analyses results for IN100, incorporating ZAF corrections for the unanalyzed elements 3.2Mo, 0.8V, 0.06C, 0.02B, and 0.06Zr, *-grain boundary point.

Analysis Point	Al	Ni	Co	Cr	Ti	Totals
1	5.101	53.847	19.822	13.705	3.769	100.384
2	5.102	54.503	19.750	13.305	4.012	100.813
3	5.166	54.258	19.923	13.538	3.954	100.980
4	5.147	54.062	19.714	13.482	4.112	100.657
5	5.153	54.640	19.763	13.291	4.120	101.106
6	5.073	53.936	20.001	13.586	3.759	100.496
* 7	4.978	53.567	20.175	13.730	3.664	100.253
* 8	5.007	53.791	20.148	13.795	3.760	100.642
9	5.075	54.358	19.872	13.491	3.870	100.807
10	5.141	54.192	19.917	13.608	3.968	100.967
11	5.091	54.420	19.609	13.287	4.069	100.617
12	5.089	54.994	19.624	13.284	4.113	101.245
* 13	4.986	53.345	20.534	14.307	3.661	100.972
* 14	5.004	53.622	20.523	14.250	3.750	101.289
* 15	5.153	54.416	19.829	13.477	3.864	100.880
16	5.749	57.159	17.818	10.623	5.254	100.743
* 17	4.918	52.406	19.897	13.640	4.680	99.681
18	6.003	59.479	17.059	9.203	5.576	101.461
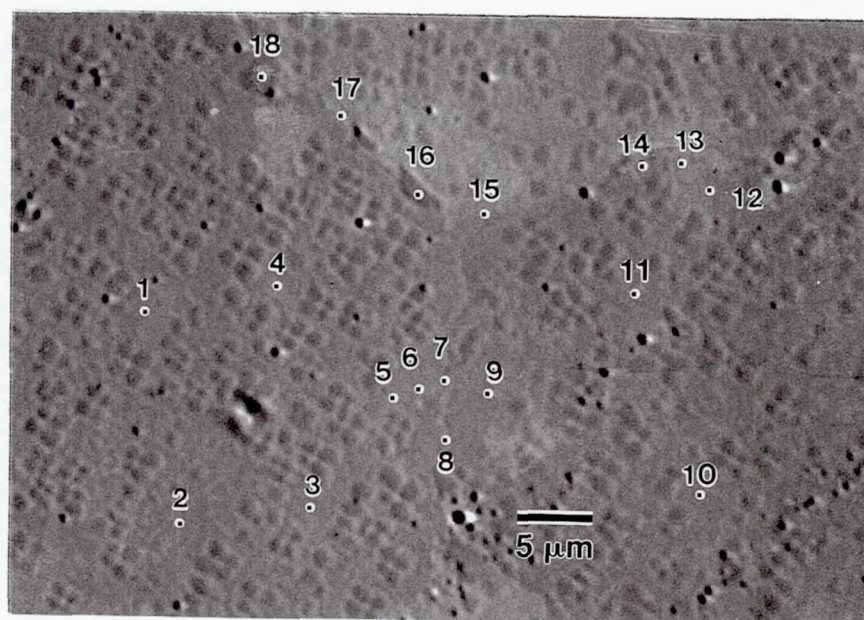
Fig. 5 (cont.) d. BSE image with the locations of quantitative point analyses.

REPORT DOCUMENTATION PAGE

1. AGENCY USE ONLY (Leave blank)	2. REPORT DATE	3. REPORT TYPE AND DATES COVERED
	January 2001	Technical Memorandum

4. TITLE AND SUBTITLE

Microprobe Evaluations of Grain Boundary Segregation in KM4 and IN100

5. FUNDING NUMBERS

WU–714–04–10–00

6. AUTHOR(S)

T.P. Gabb and J.W. Smith

7. PERFORMING ORGANIZATION NAME(S) AND ADDRESS(ES)

National Aeronautics and Space Administration
John H. Glenn Research Center at Lewis Field
Cleveland, Ohio 44135–3191

8. PERFORMING ORGANIZATION REPORT NUMBER

E–12574

9. SPONSORING/MONITORING AGENCY NAME(S) AND ADDRESS(ES)

National Aeronautics and Space Administration
Washington, DC 20546–0001

10. SPONSORING/MONITORING AGENCY REPORT NUMBER

NASA TM—2001-210666

12a. DISTRIBUTION/AVAILABILITY STATEMENT

Unclassified - Unlimited
Subject Category: 26   Distribution: Nonstandard

Available electronically at http://gltrs.grc.nasa.gov/GLTRS

This publication is available from the NASA Center for AeroSpace Information, 301–621–0390.

12b. DISTRIBUTION CODE

13. ABSTRACT (Maximum 200 words)

Turbine disk alloys subjected to fatigue cycles with dwells at high temperatures and stresses can fail by cracking along grain boundaries. This could be due to concentrated creep deformation or environmental attack at grain boundaries. It would be important to identify any chemical segregation along grain boundaries to aid understanding of this intergranular failure mode. The objective of this study was to evaluate the degree of chemical segregation present at the grain boundaries of two disk alloys, KM4 and IN100. An electron microprobe employing wavelength dispersive x-ray chemical analyses was used to characterize the chemistry along multiple grain boundaries in metallographically prepared samples of each alloy. Some degrees of boron, chromium, and cobalt enrichment of grain boundaries were observed in each alloy.

14. SUBJECT TERMS

Superalloys; Disks; Grain boundaries; Segregation

15. NUMBER OF PAGES

24

16. PRICE CODE

A03

17. SECURITY CLASSIFICATION OF REPORT	18. SECURITY CLASSIFICATION OF THIS PAGE	19. SECURITY CLASSIFICATION OF ABSTRACT	20. LIMITATION OF ABSTRACT
Unclassified	Unclassified	Unclassified	